ISSN 1674-1056
http://cpb.iphy.ac.cn
http://iopscience.iop.org/cpb
中国物理 B
Chinese Physics
中国物理
Chinese Physics B

Atomistic simulations of the lubricative mechanism of a nano-alkane lubricating film between two layers of Cu-Zn alloy

Jing Li(李京), Peng Zhu(朱鹏), Yuan-Yuan Sheng(盛圆圆), Lin Liu(刘麟), and Yong Luo(罗勇)
Citation: Chin. Phys. B, 2021, 30 (**8**): 080205. DOI: 10.1088/1674-1056/abfbd6
Journal homepage: http://cpb.iphy.ac.cn; http://iopscience.iop.org/cpb

What follows is a list of articles you may be interested in

Effect of the potential function and strain rate on mechanical behavior of the single crystal Ni-based alloys: A molecular dynamics study

Qian Yin(尹倩), Ye-Da Lian(连业达), Rong-Hai Wu(巫荣海), Li-Qiang Gao(高利强), Shu-Qun Chen(陈树群), and Zhi-Xun Wen(温志勋)
Chin. Phys. B, 2021, 30 (**8**): 080204. DOI: 10.1088/1674-1056/abff22

Growth mode of helium crystal near dislocations in titanium

Bao-Ling Zhang(张宝玲), Bao-Wen Wang(王保文), Xue Su(苏雪), Xiao-Yong Song(宋小勇), Min Li(李敏)
Chin. Phys. B, 2018, 27 (**6**): 060205. DOI: 10.1088/1674-1056/27/6/060205

Temperature dependence of migration features of self-interstitials in zirconium

Rui Zhong(钟睿), Qing Hou(侯氢), Chao-Qiong Ma(马超琼), Bao-Qin Fu(付宝勤), Jun Wang(汪俊)
Chin. Phys. B, 2017, 26 (**12**): 120202. DOI: 10.1088/1674-1056/26/12/120202

An intermediate state of T7 RNA polymerase provides another pathway of nucleotide selection

Zhan-Feng Wang(王展峰), Yu-Ru Liu(刘玉如), Peng-Ye Wang(王鹏业), Ping Xie(谢平)
Chin. Phys. B, 2017, 26 (**10**): 100203. DOI: 10.1088/1674-1056/26/10/100203

Brownian ratchet mechanism of translocation in T7 RNA polymerase facilitated by a post-translocation energy bias arising from the conformational change of the enzyme

Zhan-Feng Wang(王展峰), Zhi-Qiang Zhang(张志强), Yi-Ben Fu(付一本), Peng-Ye Wang(王鹏业), Ping Xie(谢平)
Chin. Phys. B, 2017, 26 (**3**): 030201. DOI: 10.1088/1674-1056/26/3/030201

Atomistic simulations of the lubricative mechanism of a nano-alkane lubricating film between two layers of Cu–Zn alloy*

Jing Li(李京)[1,2], Peng Zhu(朱鹏)[1,2], Yuan-Yuan Sheng(盛圆圆)[1,2], Lin Liu(刘麟)[1,2,†], and Yong Luo(罗勇)[3]

[1] School of Mechanical Engineering and Rail Transit, Changzhou University, Changzhou 213164, China
[2] Jiangsu Key Laboratory of Green Process Equipment, Changzhou University, Changzhou 213164, China
[3] School of Materials Science and Physics, University of Mining and Technology, Xuzhou 221116, China

(Received 19 January 2021; revised manuscript received 16 April 2021; accepted manuscript online 27 April 2021)

We describe simulations of lubrication by a hexadecane molecular lubricating film during the shearing process of a Cu–Zn alloy performed using the atomistic method. The results indicate that with increasing Zn contents, the interface slip between the alloy wall and the lubricating film first decreases and then increases, according to variations of the radius distribution function (RDF), while the interface slip reaches its lowest value of 0.12 during the shearing of CuZn30 alloy. We also discuss the relationship between interface roughness and the lubricating film. During film lubrication, the interface's roughness effectively inhibits interfacial slip. For the convex contact model, the presence of the hexadecane lubricating film reduces the interfacial contact pressure from 11.9 GPa to 8.7 GPa and the friction coefficient from 0.81 to 0.52.

Keywords: molecular dynamic simulation, nanotribology, Cu–Zn alloy, interface slip

PACS: 02.70.Ns, 68.35.Af, 68.35.−p, 73.43.Cd **DOI:** 10.1088/1674-1056/abfbd6

1. Introduction

Due to its excellent properties of heat conduction, electrical conduction, and wear and fatigue resistance, Cu–Zn alloy has broad application prospects in manufacturing fields such as mechanical equipment transmission and braking.[1–4] However, some research results have shown that fatigue damage to mechanical parts caused by alternating loads accounts for 50%–90% of the service process.[5] Fatigue failure generally begins on the material's surface; friction and lubrication are macro-dynamic behaviors of the material's surface. The surface morphology of Cu matrix composites has a large impact on their mechanical and lubricative properties.[6] Therefore, it is of practical significance to explore the frictional and lubricative behaviors of the surfaces of alloys. In particular, with the progress of micro-precision machinery and nanotechnology, increased lubrication requirements have been proposed. From micron-scale thin films to nanoscale lubricating-film properties, this has gradually become a research focus. Based on experimental research, some scholars have used comprehensive analysis methods to study macroscopic frictional and lubricative phenomena. However, nano-lubricating films have a different series of phenomena from macroscopic lubricating films when the friction pair gap is at the nanometer scale. This is because the flow scale of the lubricating film is similar to the mean free path of a molecule, so the conventional continuous-medium hypothesis ceases to be applicable. In addition, the relative importance of various flow forces, such as inertial force, viscous force, surface force, and volume force is changed due to the reduction of scale.[7,8] Therefore, it is necessary to study the phenomena of lubrication and friction, and explain their mechanisms at the microscopic or atomic levels.

Previous researchers have used MD methods to address various problems at the microscopic level. Ta *et al.*[9,10] studied hexadecane films confined on the surfaces of different types of iron and iron oxides. Their results showed that interfacial slip becomes severe with an increase in the loading pressure and shear rate, but that it is insensitive to temperature. The shear stress increases with an increase in the loading pressure, whereas the coefficient of friction shows a contrasting propensity. Koike and Yoneyah[11] discussed the interfacial slip of alkane molecules with chain lengths from 6 to 80 under different pressures. Tartaglino *et al.*[12] probed the lubricating effect of n-butane and isobutane on curved surfaces; the results indicated that n-butane can effectively protect metal surfaces when used for thin-film lubrication. Savio *et al.*[13] considered the effect of the interfacial slip phenomenon for lubricating films with chain lengths ranging from n-pentane to n-hexadecane. Their study showed that as the molecular chain length increases, the interfacial slip phenomenon becomes more obvious. Jabbarzadeh and Gupta[14,15] probed the influence of alkane molecular branching on the interfacial slip phenomenon, and reached the conclusion that the degree of interface slip increased with an increase in molecular branching. Mendona *et al.*[16] probed the frictional properties of ionic lubricant film in nanostructures; the friction factors obtained were consistent with experimental results. Suwa *et al.*[17] concluded that a solid surface with regularly arranged nano-slit

*Project supported by the Natural Science Foundation of Jiangsu Higher Education Institutions (Grant No. 17KJA460002) and the "Six Talent Peaks" of Jiangsu Province, China (Grant No. GDZB-002).

†Corresponding author. E-mail: liulin@cczu.edu.cn

© 2021 Chinese Physical Society and IOP Publishing Ltd

structures increases the adsorption of lubricant molecules, and that the surface nanostructure affects the adsorption characteristics and tribological characteristics.

In general, previous scholars have only considered the influence of common factors, such as the chain length and the structure of the lubricating film, on lubrication. However, the influence of solid interface properties on lubrication has not been explored in detail. Hence, in this study, the molecular dynamics simulation method was utilized to explore the relationship between alloy interfacial properties and lubricating film. The interface adsorption layer and stratification phenomenon were systematically analyzed. The effect of the Zn content of the alloy on the lubricating film's interfacial slip was studied. Additionally, by considering the relationship between the interfacial roughness and the lubricating film, the interfacial slip was thoroughly analyzed. Finally, the deformation pressure relationship between the lubricating film and the interface was revealed by the convex peak contact model.

2. Simulation and method

2.1. Model setup

N-hexadecane is the principal component of the base oil in conventional lubricating films, and the study of its tribological properties has practical significance; it has excellent thermal stability and low-temperature fluidity. The Visualizer module was used to construct hexadecane molecules, and their geometry was optimized using the Smart Minimizer method. Using the Amorphous Cell tool in Material Studio (MS), 60 hexadecane molecules of lubricating film were packed into a cell at a predefined density of 0.836 g/cm^3.[18] As shown in Fig. 1(a), face-centered cubic (FCC) structured crystalline Cu was set up as the unit cell, and expanded in the x, y, and z directions to obtain Cu walls with sizes of 30 Å, 30 Å, and 15 Å, respectively. Cu–Zn alloys with different Zn contents were constructed by randomly replacing Cu atoms with Zn atoms, according to ratio. It can be seen from Fig. 1(b) that a three-layer structured model consisting of a Cu–Zn wall, the lubricating film, and another Cu–Zn wall was built along the

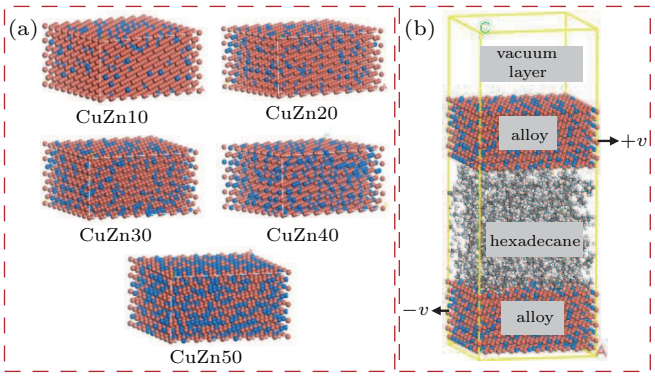


Fig. 1. (a) Cu–Zn wall with 10%, 20%, 30%, 40%, and 50% Zn contents, respectively; (b) initial configuration of the alloy (CuZn30) and the hexadecane lubricating film.

z-axis; a vacuum layer with a thickness of 20 Å was added to the top. Periodic boundary conditions were adopted in the x and y directions. The length a, width b, and height c of the model were 30 Å, 30 Å, and 69.7 Å, respectively.

2.2. Simulation steps

In this study, the all-atom molecular dynamics simulation method called the condensed phase optimized potentials for atomistic simulation studies (COMPASS) force field[19] was adopted, and this force field proved to be applicable to describing the tribological properties of the polymer, as shown below:

$$E_{\text{total}} = E_{\text{bond}} + E_{\text{angle}} + E_{\text{torsion}} + E_{\text{inversion}} + E_{\text{cross}} + E_{\text{electrostatic}} + E_{\text{vdw}}, \quad (1)$$

where E_{bond} represents the bond stretching energy, E_{angle} is the angle bending energy, E_{torsion} represents the torsional angle energy, E_{cross} represents the inversion, and E_{cross} represents the cross energy. The last two energies are non-bonded interactions: $E_{\text{electrostatic}}$ and E_{vdw} are due to the electrostatic interaction and the van der Waals interaction, respectively.

The optimized steps and important parameters are summarized in Table 1. The non-bonding truncation of the electrostatic effect and the van der Waals (VDW) effect is based on the atom based method, and the cutoff distance is 1.25 nm, so the defined friction interface area is from the interface to 12.5 Å. The control functions for pressure and temperature are the Berendsen and Nose thermostat methods, respectively.

An optimization of the materials was performed. In this process, Cu–Zn alloys and lubricating film molecules were optimized and annealed to obtain a stable structure in line with the actual situation. The optimization and simulation of the model system are presented here. The simulation processes are as follows. First of all, the positions of the atoms were fixed in the wall. At the same time, the Smart Minimizer method was utilized to optimize the geometry of the system. Second, a five-cycle annealing process was carried out at constant temperature and volume (NVT ensemble) from 300 K to 500 K for 500 ps to relax the simulated samples over a wider temperature range to obtain the minimum energy of the resultant trajectories. Importantly, the shear process set the temperature to 298 K and used the velocity algorithm[20] to solve the Newtonian equation of motion under the NVT ensemble. Normal loading was applied to the top layer by moving the alloy layer at a speed of 0.2 Å/ps for 500 ps under a loading of 101 MPa to simulate the friction process. After relaxation, the length a, width b, and height c of the model were 30 Å, 30 Å, and 59.1 Å. All the processes used 1.0 fs for the simulation time step. The total simulation time was 1500 ps, and the final 500 ps trajectory file was utilized to analyze the calculation results.

Table 1. Important parameters of the simulations.

	Step	Algorithm	Convergence criterion	Temperature (K)	Time (ps)
Optimization of materials	geometry optimization	Smart	10^{-5} kcal/mol (energy)	298	500
	anneal	Nose thermostat	–	300–500	500
Optimization of system	geometry optimization	Smart	10^{-5} kcal/mol (energy)	298	500
	anneal	Nose thermostat	–	300–500	500
	confined shear	Andersen thermostat	2×10^{-5} kcal/mol (energy)	298	500

3. Results and discussion

3.1. Lubricating film and alloy content

Figure 2 shows a snapshot of the CuZn30 wall and hexadecane lubricating film system at a shear rate of 20 m/s. It can be seen that there were several noticeable changes during the process. The hexadecane molecules are densely formed near the surface of the alloy, forming an adsorption layer with a thickness of 4 Å, as displayed by the blue area. The lubricating film changes from the random distribution of the initial model shown in Fig. 1(b) to orderly adsorption on the alloy's surface at 50 ps. Meanwhile, the red arrow represents a slight slip between the adsorption layer and the interface during the shearing process. At 150 ps, the hexadecane molecules in the adsorption layer are mostly arranged parallel to the surface.[21] In the middle area, molecules perform an isotropic irregular motion, showing a state similar to that of the bulk fluid, which is consistent with previous experimental results.[22,23]

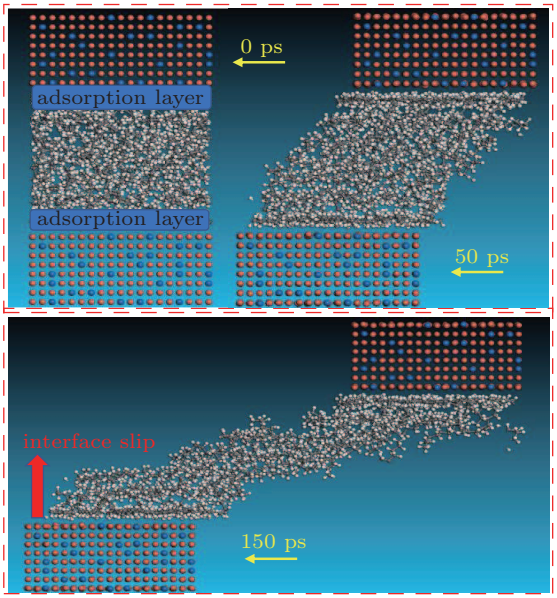


Fig. 2. Snapshots of the shear configuration of hexadecane lubricating film at 0 ps, 50 ps, and 150 ps, respectively.

The molecules of the adsorption layer can be adsorbed to the wall's surface due to the strong attraction of the alloy's atoms, while the moving Cu–Zn wall layer generates a shearing effect on the lubricating film. The reason for this is that the adsorption layer moves along with the wall's surface. As the distance between the hexadecane molecules and the wall's surface increases, the adsorption effect of the alloy atoms on these hexadecane molecules decreases. Thus, the interaction between molecular chains becomes dominant; its energy is 265.8 kcal/mol. Finally, hexadecane molecules in the middle area follow the adsorption layer molecules and flow together. The entire lubricating film forms a certain velocity gradient, presenting a state similar to a Couette fluid.[24,25]

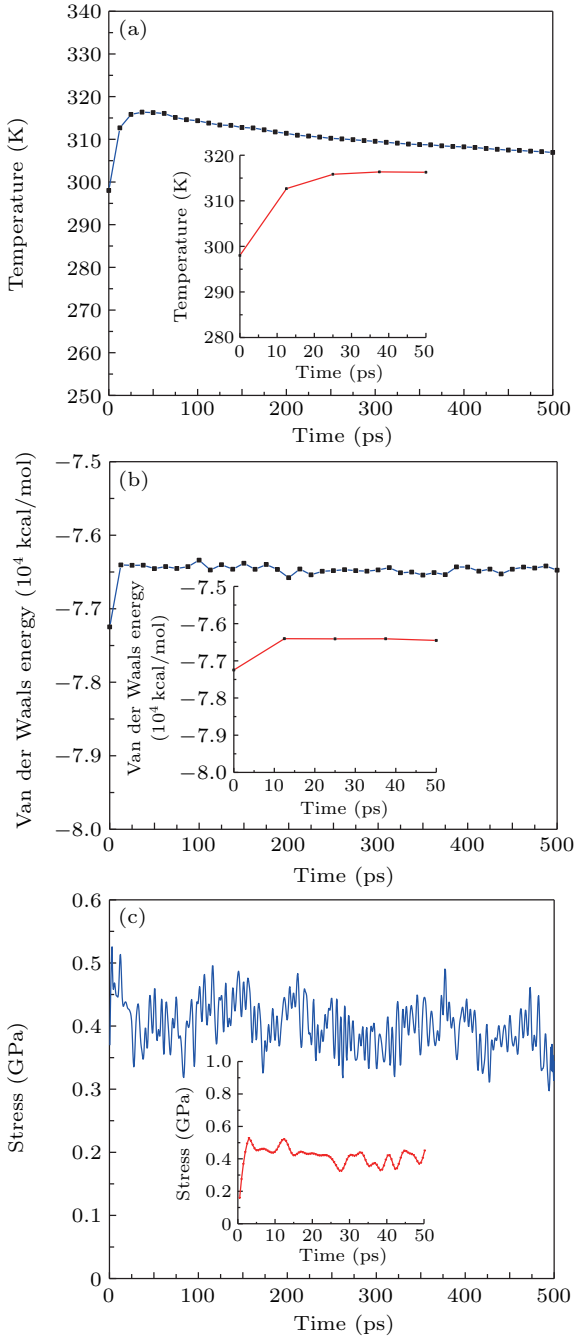


Fig. 3. The (a) temperature, (b) van der Waals energy, and (c) stress during shear process.

Figure 3 shows the stress, temperature, and VDW energy curves of the shearing process over time to confirm the detailed characteristics of the adsorption layer. It is clear that the values of temperature, VDW energy, and stress increase at the beginning of the process, which indicates that the lubricating film is adsorbed. The stress, temperature, and VDW energy of the lubricating film are constant after 50 ps, which indicates a normal shearing process between the alloy and the lubricating film.

The lubricating film's structural properties change significantly when the system reaches nanometer size. The salient feature is that the lubricating film tends to form an adsorption layer near the solid boundary. Figure 4(a) shows the relative concentration distribution inside the lubricating film of the CuZn30 alloy at a shear rate of 20 m/s. The relative concentration exhibits seven peaks with increasing film thicknesses, which means that the internal lubricating film is stratified into seven layers. It can be seen that the relative concentration has a high value at the interfaces between the alloy and the lubricating film atoms at about 18 Å and 42 Å. Because the hexadecane molecules exhibit an adsorptive behavior on the surface of the Cu–Zn alloy, the relative concentration of molecules near the wall is quite high. Figure 4(b) shows a layered structural diagram of the hexadecane lubricating film with the CuZn30 alloy, which also intuitively shows the delamination phenomenon of the lubricating film, and that the molecules between the lubricating layers are connected to each other by branch chains. In the middle area of the lubricating film, there is small gap in the values of the relative concentration, which means that certain characteristics of the liquid are still maintained.[26,27] The analysis results also confirm the formation of an adsorbed layer after analyzing the concentration distribution inside the lubricating film.

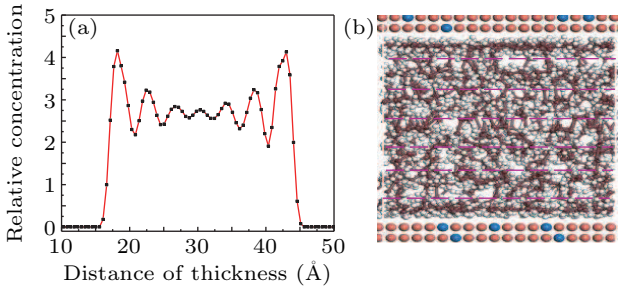


Fig. 4. (a) Relative concentration distribution between the hexadecane lubricating film and the CuZn30 alloy, (b) layered structural diagram of the hexadecane lubricating film with the CuZn30 alloy.

In order to clearly understand the stratification phenomenon caused by the relative concentration distribution in the lubricating film, the interaction energy between the alloy wall and each molecular layer of the lubricating film is presented in Table 2. The E_1 to E_4 represent the interaction energies between the alloy wall and the first to fourth layers of hexadecane molecules nearby, respectively. The negative values suggest that the Cu–Zn alloy walls and the molecular layer are mutually attracted.

Table 2. The interaction energies between the Cu–Zn wall and the lubricating film's hexadecane molecular layers.

Zn% (Cu–Zn)	E_1 (kcal/mol)	E_2 (kcal/mol)	E_3 (kcal/mol)	E_4 (kcal/mol)
10%	−1074.5	−45.7	−10.3	0
20%	−1105.1	−54.3	−14.2	0
30%	−1156.5	−69.5	−15.1	0
40%	−1131.1	−62.2	−13.2	0
50%	−1095.4	−46.7	−11.2	0

The interaction energies between the wall and the first to fourth layers of the hexadecane molecules of the lubricating film are $-1156.5 \sim 1074.5$ kcal/mol, $-69.5 \sim -45.7$ kcal/mol, $-15.1 \sim -10.3$ kcal/mol, and 0 kcal/mol, respectively. This indicates that the first layer of hexadecane molecules near the alloy wall is strongly attracted to the wall, thus forming an adsorption layer. However, the alloy wall is less attractive to the hexadecane molecular layer when the hexadecane molecular layer is far from the alloy wall. There is no attraction between the fourth layer of hexadecane molecules and the wall, which clarifies the formation of the stratification phenomenon.

3.2. Effect of Zn content on interfacial slip

When the alloy wall slides at a particular speed, the lubricating film moves with the wall's surface because of the strong attraction between the alloy wall and the lubricating film; a certain speed gradient is produced along the z-axis in the lubricating film. In order to analyze the sliding characteristics of the lubricating film, we slide the upper and lower alloy walls in the horizontal direction to form a steady-state shear flow and then calculate the flow velocity profile.

Figure 5 shows the simulation results for the velocity profile of the lubricating film at a 20 m/s shear rate for different Zn contents. The horizontal dashed lines represent the velocity of the alloy wall, and the middle part is the velocity distribution of the hexadecane film. There is an obvious relative speed between the wall and the lubricating film, which is interfacial slip. Another interesting phenomenon observed is that there is a step jump in the velocity profile between the first layer and the second layer. This indicates that layer slip occurs inside the lubricating film.[28] The flow velocity is linearly distributed in the middle of the lubricating film, which shows that the intermediate film's hexadecane molecules exhibit the velocity distribution state of a liquid fluid.

This study was intended to compare the velocity distributions of lubricating films for different Zn contents of Cu–Zn. It can be seen from Fig. 5 that the film interface velocities of CuZn10 are relatively small; its interfacial velocities are −11.3 m/s and 11.5 m/s. Then, as the Zn content in the alloy increases, the interfacial velocities also increase. The film

interface velocities of the CuZn20 alloy are −13.9 m/s and 12.9 m/s. Finally, the film interface velocities at the interface with the CuZn30 alloy reach the highest values of −17.6 m/s and 17.8 m/s, indicating that most of the molecules in the first layer still move with the wall. However, when the Zn content reaches that of CuZn40, the velocities of the film interface molecules are reduced, compared to those of CuZn30; the values are −14.6 m/s and 14.5 m/s. In the case of CuZn50 alloy lubrication, the velocities decrease further, to −12.3 m/s and 12.5 m/s.

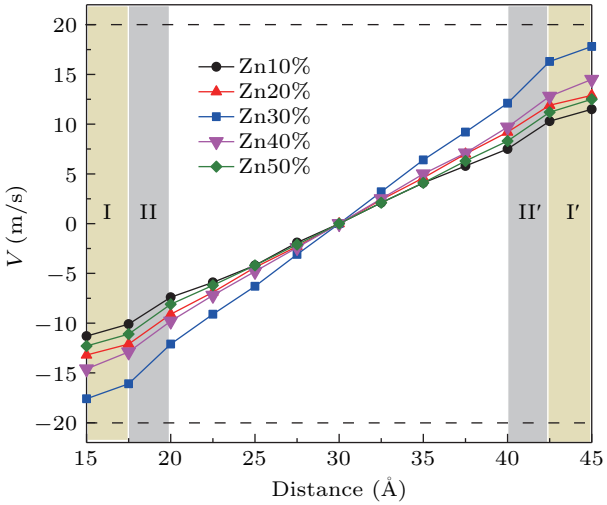


Fig. 5. Velocity distribution diagram of a hexadecane lubricating film with a thickness of 30 Å used to lubricate CuZn surfaces with varying Zn contents.

In the classic theory of hydrodynamic lubrication, fluid molecules adjacent to a solid wall are considered to move at the same velocity as the wall, which is known as the 'no-slip' boundary condition and widely used in practical fluid engineering.[29] However, there is an interfacial slip in microlubrication. The degree of interfacial slip between the wall and the lubricating film is represented by the interfacial slip factor S, whose calculation method is shown below:[30]

$$S = \frac{V_{\mathrm{w}} - V_{\mathrm{f}}}{V_{\mathrm{w}}}, \tag{2}$$

where V_{w} and V_{f} are the wall velocity and the average film interface velocity in adjacent areas of the wall, respectively. Also, V_{w} and V_{f} can be obtained from Fig. 5.

This study calculated the interface slip S of Cu–Zn alloys with different Zn contents adjacent to the film, as shown in Table 3. It is clear that when the Zn content in the alloy is 10%, the interface slip S has its largest value of 0.43. When the Zn content in the alloy is 20%, S is reduced to 0.34. When the Zn content in the alloy is 30%, S reaches its smallest value of 0.12. However, with a continued increase of the Zn content in the alloy, the S of the CuZn40 alloy reaches 0.21, and the S of the CuZn50 alloy further increases to 0.36. This shows that when the Zn content of the alloy is less than 30%, the interfacial slip associated with the Cu–Zn alloy decreases with increasing Zn content. Conversely, when the Zn content in the alloy is increased above 30%, the interfacial slip of the Cu–Zn alloy increases with increasing Zn content.

Table 3. Interfacial slip factor for different Zn% (Cu–Zn).

Alloy	CuZn10	CuZn20	CuZn30	CuZn40	CuZn50
S	0.43	0.34	0.12	0.21	0.36

In order to explore the influence of Cu–Zn alloys with different Zn contents on the interface slip S in detail, this study analyzed the internal structures of Cu–Zn alloys with different Zn contents using the RDF method. The $g(r)$ of the RDF can be interpreted as the ratio of the local area density to the average density. In other words, the RDF reflects the characteristics of the aggregation of atoms in the alloy, which helps us to understand the internal structure of the alloy.[31] The formula for the RDF is given as

$$g(r) = \frac{\mathrm{d}N}{\rho 4\pi r^2 \mathrm{d}r}, \tag{3}$$

where ρ is the density of the system and N represents the number of molecules in the system. Taking any atom as the reference atom, the number of atoms within the distance r to $r + \mathrm{d}r$ from Zn is $\mathrm{d}N$.

Figure 6 shows that the Cu–Zn alloy atoms exhibit maximum aggregation at a distance of 2.51 Å. However, by examining the different values of Zn content in the alloys, it can clearly be seen that the $g(r)$ value of Zn10% is 30.00, the $g(r)$ value of Zn20% is 30.40, and the $g(r)$ of Zn30% has the maximum value, at 30.74. Then, as the percentage of Zn content continues to increase in the alloy, it weakens the atomic aggregation: the $g(r)$ values of Zn40% and Zn50% are 30.56 and 30.13, respectively.

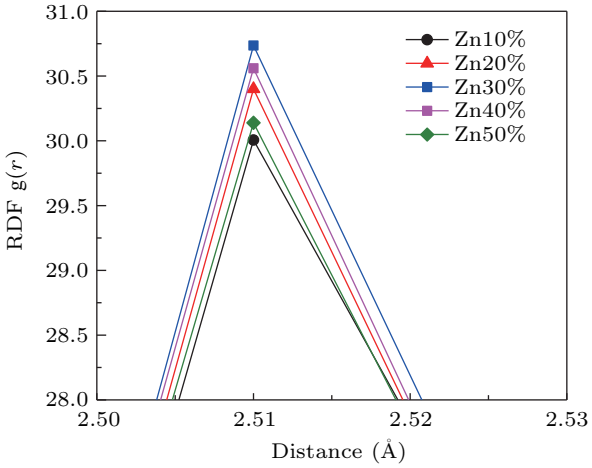


Fig. 6. Radial distribution function graph of alloys with 10%, 20%, 30%, 40% and 50% Zn (in Cu–Zn).

Figure 7 shows the RDF values of the different Cu–Zn contents compared to a H atom in the lubrication film during the shearing process, which explains the interaction between the alloy and the lubricating film.[30] The value of the interaction between the alloy and the lubricating film reaches a maximum at 2.4 Å. Different values appear because the Zn content in the alloy causes the ratio of the maximum RDF of the alloy

to the H atom in the lubrication film to be different. The RDF ratio reaches a minimum for CuZn10 versus the H atom in the lubrication film, and the ratio reaches a maximum for CuZn30 versus the H atom in the lubrication film.

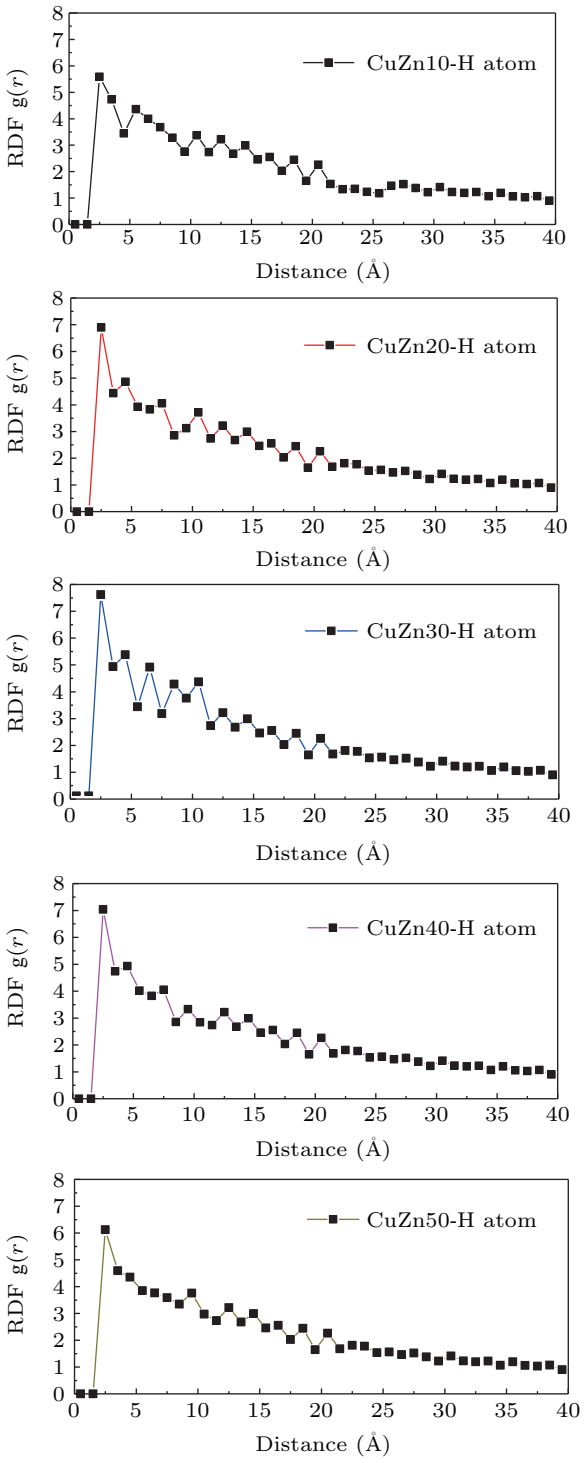


Fig. 7. RDF ratios between the Cu–Zn alloys and the H atom in the lubrication film during the shearing process.

As shown in Table 4, V represents the gap between the wall velocity and the average film interface velocity. The $g_2(r)$ values represent the RDF ratios of the different Cu–Zn alloys to H atoms in the lubrication film. E represents the energy of the interaction between the alloy wall and the lubricating film. With increasing Zn contents in the alloys, the trend of atomic aggregation $g(r)$ is consistent with those of $g_2(r)$ and E. It can be seen that increasing the Zn content changes the atomic aggregation $g(r)$ inside the alloy, resulting in an increase in $g_2(r)$ and adsorption E. The high interaction E reduces V between the lubricating film and the alloy, and ultimately leads to a small interfacial slip S. It is found that the interaction between the alloy and the lubricating film reaches a maximum when the Zn content is 30%. A subsequent increase of the Zn content reduces the interaction between the alloy wall and the lubricating film.

Table 4. The values of $g(r)$, $g_2(r)$, E, V, and S for different Zn% (in Cu–Zn).

	CuZn10	CuZn20	CuZn30	CuZn40	CuZn50
$g(r)$	30.00	30.40	30.74	30.56	30.13
$g_2(r)$	5.59	6.89	7.62	7.03	6.13
E (kcal/mol)	−1130.5	−1173.6	−1241.1	−1207.2	−1153.3
V (m/s)	8.6	6.8	2.4	4.2	7.2
S	0.43	0.34	0.12	0.21	0.36

3.3. Lubricating film and interface roughness

In practical engineering applications, roughness is an unavoidable problem. When machines and parts are examined at the micro or nanoscales, the macroscopic laws of friction break down for nanoscale contacts due to atomic-scale surface roughness. This has encouraged research into the effects of atomic roughness on lubrication and friction.[32] In order to fully understand the influence of roughness on the lubricating film in the shearing process, this study selected the CuZn10 alloy as the research object with which to explore interfacial slip. The reason for this is that the interface slip of the lubrication film is the largest for CuZn10 alloy.

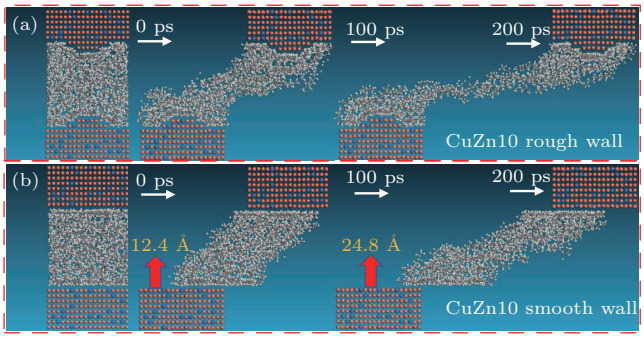


Fig. 8. (a) Simulated snapshots of the lubricating film applied to CuZn10 rough walls at 0 ps, 100 ps and 200 ps, respectively. (b) Simulated snapshots of the lubricating film applied to CuZn10 smooth walls at 0 ps, 100 ps and 200 ps, respectively.

Importantly, the lubrication state of rough CuZn10 was monitored at different stages and compared with that of smooth surfaces, as shown in Fig 8. It can clearly be seen that the lubricating film has a certain slip when applied to the smooth interface at 100 ps; the value of the interfacial slip length is 12.4 Å. However, the lubrication film applied to the rough interface did not produce interfacial slip. The figure shows that the slip length of the smooth interface has further increased at 200 ps; the value of the interfacial slip length is

now 24.8 Å. However, when comparing the internal changes of the lubricating film, it can be seen that the rough interface still has no slip.

Figure 9 shows the relative concentration of the lubricating film for rough and smooth interfaces. It can be seen that the rough interface reaches a value larger than zero earlier than the smooth interface, which indicates that hexadecane molecules have been adsorbed in the rough gaps. Comparing the middle area of the concentration distribution, it can be seen that the concentration change of the rough interface is more stable, and that the numerical value is relatively low. These results suggest that a certain degree of shear thinning occurs in the lubricating film applied to the rough interface.

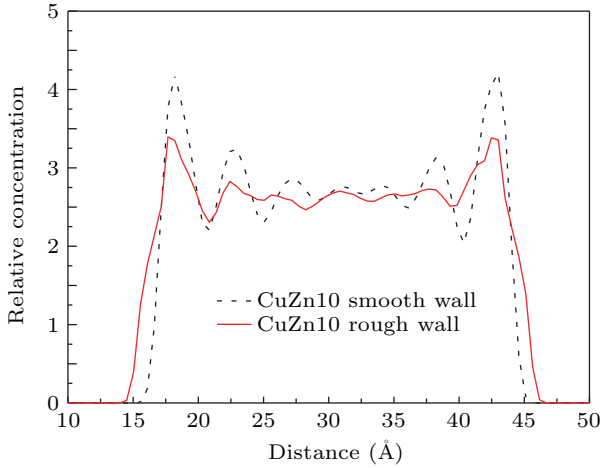


Fig. 9. Relative concentration distributions of the lubricating film applied to rough and smooth interfaces.

The degree of interfacial slip is determined by the properties of the wall, such as the attraction between the wall and the lubricating film, and the shear of the wall. When the lubricating film is weakly attracted, for example, by the CuZn10 alloy, the action of the wall shearing movement overcomes the attraction between the alloy wall and the lubricating film, forming a speed gap V with the wall's movement, and, as a result, causes the interface slip S. However, when the smooth and rough walls of the CuZn10 alloy were explored, we found that when the wall was rough, molecules were adsorbed due to the existence of gaps, as shown in Fig. 9. Although the attraction was not able to overcome the shear when the wall was sheared and moved, the protruding wall atoms hindered the interfacial slip of the hexadecane molecules in the gaps. The rough peak atoms forced the hexadecane molecules to become closer to each other. For the hexadecane molecules in the middle area, the speed of the adsorption layer of the rough wall's surface was larger than the speed of the adsorption layer of the smooth wall's surface. The middle area of the rough wall was more prone to shear thinning.

The lubricating friction changes from thin film lubrication to a convex peak contact as the thickness of the lubricating film decreases. To fully understand the change in the rough peaks during the shear process, the dry friction lubrication model and the hexadecane molecular lubrication film's friction model were compared. Except for the difference in alloy morphology (a triangular rough peak with a base length of 15 Å and a height of 12 Å), the settings for the rough interface shown in Fig. 10 are completely consistent with the settings shown in Table 1.

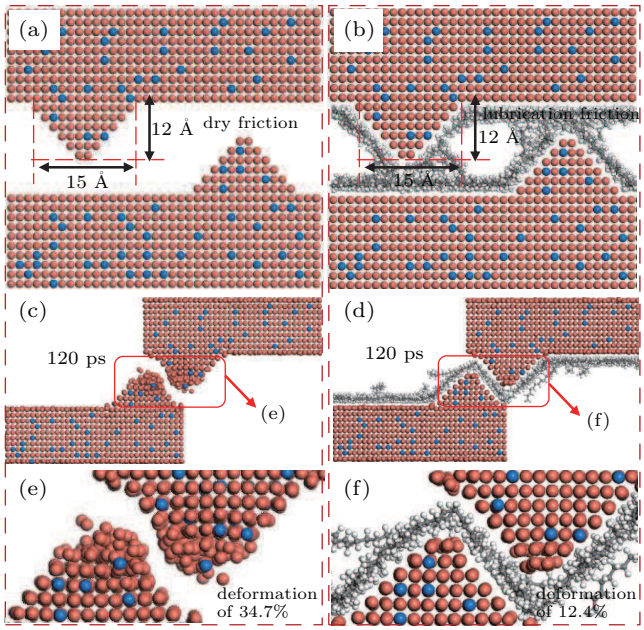


Fig. 10. (a) Optimized dry friction initial model. (b) Optimized cetane lubrication initial friction model. (c) Dry friction model simulation snapshot at 120 ps, (d) Lubricated friction model simulation snapshot at 120 ps. (e) Partial schematic diagram of the rough peak deformation of convex peak dry friction contact. (f) Partial schematic diagram of the rough peak deformation of convex peak lubricated friction contact.

The dry friction of the convex peak contact and the lubricated friction model were established using 60 hexadecane molecules. Figures 10(a) and 10(b) show the models after the geometric optimization and the annealing operation. To move the alloy and make the asperities contact, the alloy walls of the upper and lower layers were given opposing x-speeds of 20 m/s. The lubricated friction model formed an adsorption layer at the interface and presented an orderly arrangement, in agreement with Fig 2. The dry friction model and the lubricated friction model can be seen at 120 ps, respectively. Due to the contact of the rough peaks in the shearing process, it can be seen from Figs. 10(c) and 10(d) that the rough peaks of the dry friction and lubricated friction models have undergone a certain amount of deformation. We observed a partial enlargement of the rough peaks, as shown in Figs. 10(e) and 10(f). It can clearly be seen that the degree of deformation of the rough peaks in the lubricating film model was much smaller than for the dry friction model. Moreover, we calculated the deformation values for dry friction and lubricated friction. For dry friction, the convex peak deformation scale was 32.7%, and the convex peak's deformation value for lubricated friction was about 12.4%. Therefore, the hexadecane molecular

lubricant film protects the original morphology of the interfacial rough peaks to a certain extent.

To reveal the mechanisms of the lubricating film protecting the interface morphology in detail, we calculated the pressure profile and van der Waals energy during the shearing processes of dry friction and lubricated friction, as shown in Fig 11. The VDW energies of the dry friction model and the lubricated friction model were −433983.9 kcal/mol and −437215.1 kcal/mol at 0–60 ps, respectively, because the rough peaks of the alloy wall had not yet been contacted, and the VDW energy remained constant during the process. At 60 ps, the stress force abruptly decreased and a negative value was observed, while the VDW energy decreased. The reason for this was the close approach of the surface atoms of the upper and lower rough peaks, which exhibited the characteristic of mutual attraction. As the shearing process progressed, interfacial pressure started to appear and kept increasing; then, the rough peak was deformed at 60–100 ps and the VDW energy increased when the alloy atoms were in frictional contact. After 10 ps, the rough peaks ceased contact completely.

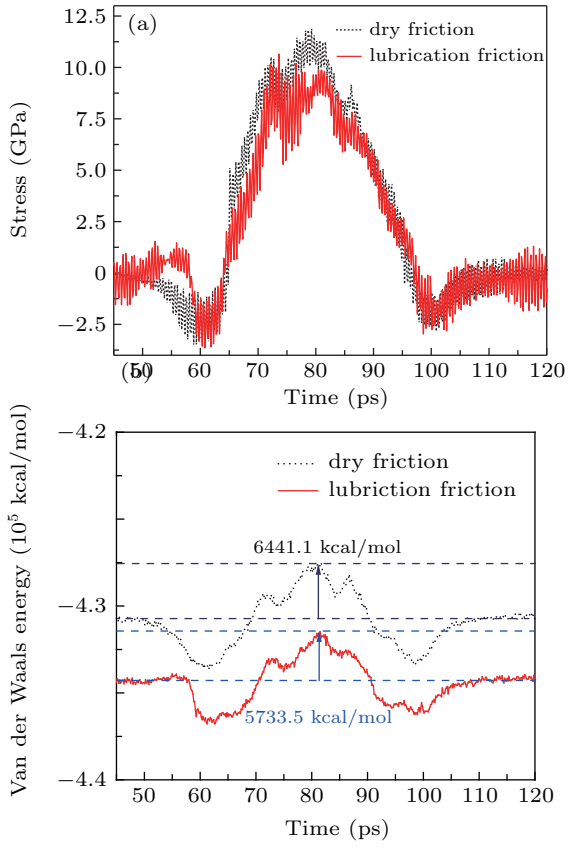


Fig. 11. Interfacial pressure (a) and van der Waals energy (b) over time from 45–120 ps.

Figure 12 shows simulated snapshots of dry friction and lubricated friction at 80 ps. At this point, the upper and lower interfaces of the model were completely in contact. At the same time, the interfacial pressures of dry friction and lubricated friction reached maxima of 11.9 GPa and 8.7 GPa, respectively.[33,34] Compared with the dry friction system, the maximum pressure of the lubricated friction was reduced by 26.8%. Also, the VDW energies of dry friction and lubricated friction also reached maximum values, which were −427542.8 kcal/mol and −431481.6 kcal/mol, respectively. Compared with the initial VDW energy, the dry friction model increased the VDW energy by 6441.1 kcal/mol during the friction process and the lubricated friction model increased the VDW energy by 5733.5 kcal/mol. The dry friction generated more energy than the lubricated friction, which indicates that the presence of the lubricating film reduced the pressure between the rough peaks during the shearing process, thereby reducing the degree of deformation of the rough peaks and protecting the interface morphology.

Moreover, Fig. 13 shows the variation of the friction coefficients of dry friction and lubricated friction. It is clear that at the previous stage of convex peak contact, the friction coefficient with lubrication is larger than that of dry friction, due to the early contact caused by the presence of the lubricating film. However, the friction coefficient of lubricated friction is smaller than that of dry friction during the main contact time of the rough peaks. In addition, the friction coefficient of dry friction fluctuates around 0.81, while the friction coefficient of lubricated friction is about 0.52, which suggests that the presence of the lubricating film reduces the friction coefficient.

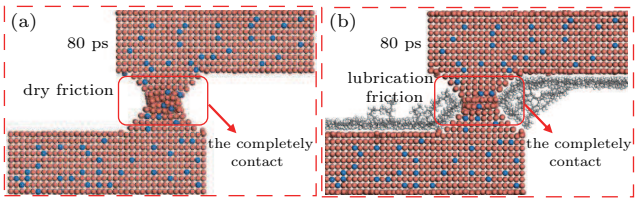


Fig. 12. (a) Dry friction vs. (b) lubricated friction at 80 ps (simulation snapshot).

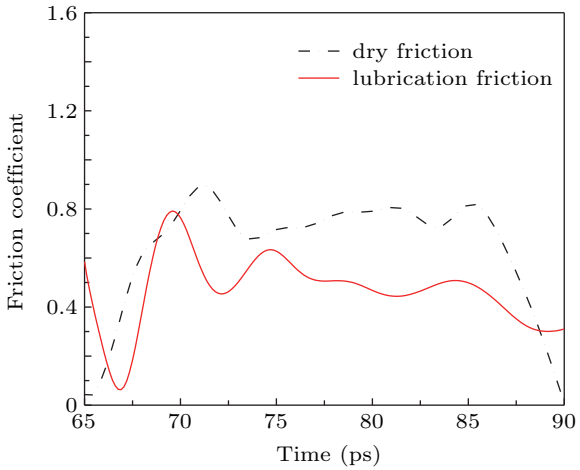


Fig. 13. Variation of the friction coefficients of dry friction and lubricated friction.

4. Conclusion

In this study, MD simulations were used to investigate the lubricated shear processes of a hexadecane molecular lubricating film applied to CuZn alloy walls, which revealed the

inherent mechanisms of the lubricating film and the alloys at an atomic level. We draw the following conclusions:

(i) From our analysis of the relative concentration of the lubricating film and our calculation of the interface adsorption energy, the results suggest that the lubricating film forms a solid-type layer at the interface, while still maintaining fluid characteristics in the middle.

(ii) The Zn content of the alloy affected the adsorption of the interface with the lubricating film. The RDF values indicate that increasing the Zn content increases the adsorption of the lubricating film, and finally inhibits the interfacial slip. The interfacial slip reaches its smallest value of 0.12 between CuZn30 and the hexadecane molecular lubricating film.

(iii) The relationships between the interfacial roughness and the lubricating film were explored. In the film lubrication model, the interface roughness greatly inhibited the interface slip of the lubricating film. In the convex peak contact model, the lubricating film reduced the interface pressure from 11.9 GPa to 8.7 GPa and reduced the friction coefficient from 0.81 to 0.52.

References

[1] Liu L, Sheng Y Y, Zhan P J, Chi R and Zhou J Z 2019 *The Chinese Journal of Nonferrous Metals* **29** 295
[2] Lu H T 2011 *Manufacturing Automation* **33** 130
[3] Gazizov M and Kaibyshev R 2017 *Transactions of Nonferrous Metals Society of China* **27** 1215
[4] Tang K, He C, Huang Q, Huang Z Y, Wang C, Wang Q Y, Liu Y J and Zhong B 2017 *International Journal of Fatigue* **99** 35
[5] Alemdag Y and Beder M 2019 *Transactions of Nonferrous Metals Society of China* **29** 2463
[6] Silvain JF, Heintz JM, Veillere A, Constantin L and Lu Y F 2020 *International Journal of Extreme Manufacturing* **2** 012002
[7] Guo Z Y and Li Z X 2003 *International Journal of Heat and Mass Transfer* **46** 149
[8] Guo Z Y and Li Z X 2003 *International Journal of Heat and Fluid Flow* **24** 284
[9] Ta T D, Tieu A K, Zhu H, Kosasih B, Zhu Q and Phan H T 2017 *Tribology International* **113** 26
[10] Deng G Y, Tieu A K, Su L H, Zhu H T, Zhu Q, Zamri W F H and Kong C 2019 *International Journal of Mechanical Sciences* **155** 267
[11] Koike A and Yoneya M 1998 *J. Phys. Chem. B* **102** 3669
[12] Tartaglino U, Sivebaek I M, Persson B M J and Tosatti E 2006 *J. Chem. Phys.* **125** 014704
[13] Savio D, Fillot N, Vergne P and Zaccheddu M 2012 *Tribology Letters* **46** 11
[14] Gupta S A, Cochran H D and Cummings P T 1997 *J. Chem. Phys.* **107** 10327
[15] Jabbarzadeh A, Atkinson J D and Tanner R I 2002 *Tribology International* **35** 35
[16] Suwa T, Ueki Y and Shibahara M 2018 *Computers & Fluids* **164** 12
[17] Mendona A C F, Agílio A, Pádua H and Malfreyt P 2013 *Journal of Chemical Theory & Computation* **9** 1600
[18] Dong P L, Lv Q, Wang W J, Chen S H, Li C L, Sun S Q and Hu S Q 2015 *Tribology* **35** 665
[19] Sun H J 1998 *J. Phys. Chem. B* **102** 7338
[20] Paterlini M G and Ferguson D M 1998 *Chemical Physics* **236** 243
[21] Tsige M and Patnaik S S 2008 *Chemical Physics Letters* **457** 357
[22] Montfort J P and Hadziioannou G 1988 *J. Chem. Phys.* **88** 7187
[23] Ranick S 1991 *Science* **253** 1374
[24] Wendl M C 1999 *Phys. Rev. E* **60** 6192
[25] Zhang X J, Huang Y, Guo Y B, Tian Y and Meng Y G 2013 *Chin. Phys. B* **22** 016202
[26] Wang S, Pan L and Li Q 2013 *Applied Polymer Science* **130** 2523
[27] Cieplak M, Koplik J and Banavar J 2001 *Phys. Rev. Lett.* **86** 803
[28] Manias E, Hadziioannou G, Bitsanis I and Brinke G T 1993 *Europhys. Lett.* **24** 99
[29] Zhang K K 1994 *Journal of Fluid Mechanics* **268** 211
[30] Wang H, Hu Y Z and Guo Y Y 2004 *Lubrication Science* **16** 303
[31] Song J and Zhao G 2019 *Tribology International* **136** 234
[32] Zheng X, Zhu H T, Kiet Tieu A and Kosasih B 2013 *Tribology International* **67** 217
[33] Erdemir A, Ramirez G, Eryilmaz O L and Sankaranarayanan S K R S 2016 *Nature* **536** 67
[34] Zhang X Y, Lu B, Wu Y H, Zhang K and Yan T T 2019 *Lubrication Engineering* **44** 83